Research Article

Maryam Musleh Althobiti, Badr Alzahrani, Abozer Y. Elderdery*, Nasser A. N. Alzerwi, Musaed Rayzah, Ahmed M. E. Elkhalifa, Bandar Idrees, Ebtisam Bakhsh, Abdulrahim A. Alabdulsalam, A. Mohamedain, Suresh S. Kumar, and Pooi Ling Mok

In vitro anti-cancer and antimicrobial effects of manganese oxide nanoparticles synthesized using the *Glycyrrhiza uralensis* leaf extract on breast cancer cell lines

https://doi.org/10.1515/gps-2023-0063
received April 08, 2023; accepted July 03, 2023

Abstract: In this study, we evaluated the antiproliferative and apoptotic properties of Pluronic-F127-containing manganese oxide nanoparticles (PF-127-coated Mn_2O_3 NPs) derived from the leaf extract of *Glycyrrhiza uralensis* (GU) on breast adenocarcinoma, MCF7, and MDA-MB-231 cell lines. The leaf extract of GU contains bioactive molecules that act as a reducing or capping agent to form Mn_2O_3 NPs. Various analytical techniques were used to characterize the physiochemical properties of PF-127-coated Mn_2O_3 NPs, including spectroscopy (ultralight-Vis, Fourier transform infrared, photoluminescence), electron microscopy (field emission scanning electron microscopy and transmission electron microscopy), X-ray diffraction (XRD), electron diffracted X-ray spectroscopy (EDAX), and dynamic light scattering. The average crystallite size of Mn_2O_3 NPs was estimated to be 80 nm, and the NPs had a cubic crystalline structure. PF127-encapsulated Mn_2O_3 NPs significantly reduce MDA-MB-231 and MCF-7 cell proliferation, while increasing endogenous ROS and lowering mitochondrial matrix protein levels. DAPI, EtBr/AO dual staining, and Annexin-V-FITC-based flow cytometry analysis revealed that PF127-coated Mn_2O_3 NP-treated breast cancer cells exhibit nuclear damage and apoptotic cell death, resulting in cell cycle arrest in the S phase. Furthermore, PF127-encapsulated Mn_2O_3 NPs show strong antimicrobial efficacy against various strains. As a result, we can conclude that PF127-coated Mn_2O_3 NPs may be effective as future anticancer agents and treatment options for breast cancer.

Keywords: Pluronic F-127, manganese oxide nanoparticles, *Glycyrrhiza uralensis* leaf extract, breast cancer, anticancer

*** Corresponding author: Abozer Y. Elderdery,** Department of Clinical Laboratory Sciences, College of Applied Medical Sciences, Jouf University, Sakaka, Saudi Arabia, e-mail: ayelderdery@ju.edu.sa
Maryam Musleh Althobiti: Department of Clinical Laboratory Sciences, College of Applied Medical Sciences, Shaqra University, Shaqra, Saudi Arabia
Badr Alzahrani: Department of Clinical Laboratory Sciences, College of Applied Medical Sciences, Jouf University, Sakaka, Saudi Arabia
Nasser A. N. Alzerwi, Musaed Rayzah: Department of Surgery, College of Medicine, Majmaah University, P. O. Box 66, Al-Majmaah 11952, Riyadh, Kingdom of Saudi Arabia
Ahmed M. E. Elkhalifa: Department of Public Health, College of Health Sciences, Saudi Electronic University, Riyadh, Kingdom of Saudi Arabia; Department of Haematology, Faculty of Medical Laboratory Sciences, University of El Imam El Mahdi, Kosti, Sudan
Bandar Idrees: Department of Surgery, Prince Sultan Military Medical City in Riyadh, Makkah Al Mukarramah Rd, As Sulimaniyah, Saudi Arabia
Ebtisam Bakhsh: Clinical Sciences Department, College of Medicine, Princess Nourah Bint Abdulrahman University, Riyadh, Saudi Arabia
Abdulrahim A. Alabdulsalam: Department of Biomedical Sciences, College of Medicine, King Faisal University, Alhofuf, Saudi Arabia
A. Mohamedain: Department of Biomedical Sciences, College of Medicine, King Faisal University, Alhofuf, Saudi Arabia; Department of Biochemistry, Faculty of Medicine, Khartoum University, Khartoum, Sudan
Suresh S. Kumar: Centre for Materials Engineering and Regenerative Medicine, Bharath Institute of Higher Education and Research, Chennai, India
Pooi Ling Mok: Department of Biomedical Sciences, Faculty of Medicine and Health Sciences, Universiti Putra Malaysia, 43400 UPM Serdang, Selangor, Malaysia
ORCID: Abozer Y. Elderdery 0000-0002-6219-5312

1 Introduction

Nanotechnology involves the science, engineering, and manipulation of nanoscale materials and devices, aiming to develop improved characteristics and innovative properties. Nanoparticles (NPs) are extensively employed and applicable in a variety of industries, such as chemical, medical, automotive, healthcare, cosmetics, and energy [1]. NPs, small particles with high surface area-to-volume

ratios, have potential applications in biological, catalytic, mechanical, and electroconductivity. Metal oxide NPs have higher surface area and volume ratios than bulk materials, making them suitable for antibacterial and cancer treatments [2].

Green nanotechnology is a key component of clean technologies intended to preserve the environment and transform supplemental bioactive components into more economical and environmentally beneficial green nanomaterials [3]. Green chemistry utilizes plant extracts to reduce and stabilize manganese metal into NPs, offering scalability, medical applications, and biocompatibility [4,5]. Eco-friendly, sustainable, cost-effective, and simple, this process outperforms conventional chemical-based techniques [6].

Green nanotechnology focuses on the environmentally friendly, sustainable development and utilization of nanomaterials, minimizing environmental and health risks while maximizing benefits. It involves eco-friendly synthesis methods, renewable materials, and environmentally benign approaches throughout their lifecycles [7]. Metallic NPs, including silver, gold, copper, iron oxide, and zinc oxide NPs, have attracted considerable attention in nanotechnology due to their unique properties and versatile applications [8]. These NPs possess distinctive physicochemical properties, such as a large surface-to-volume ratio, quantum confinement effects, and localized surface plasmon resonance, which make them attractive for a wide range of applications [9]. Nanotechnology, including green and metallic NPs, advances pharmaceutical and biomedical fields. It improves drug delivery, imaging, diagnostics, therapeutics, tissue engineering, and cancer treatment. Further research and development can improve healthcare and address biomedical challenges [10].

Green synthesis of Mn_2O_3 NPs offers several advantages over traditional physical and chemical synthesis methods. Here are some green synthesis advantages: green synthesis methods utilize natural and renewable resources, such as plant extracts, as reducing and stabilizing agents. This reduces the dependence on hazardous chemicals and minimizes the generation of toxic by-products, making it an eco-friendly approach [11]. Green synthesis methods often use low-cost starting materials and simple reaction conditions, making the overall process more cost-effective than traditional methods requiring expensive reagents and complex equipment [12]. Green synthesis methods generally operate under ambient or mild reaction conditions, such as room temperature and atmospheric pressure. This saves energy and preserves the bioactivity and stability of synthesized NPs [13]. Green-derived Mn_2O_3 NPs are typically made with biocompatible and biodegradable materials, making them suitable for various biomedical applications. These NPs can be used in drug delivery, imaging, diagnostics, and therapeutic applications with reduced toxicity and improved biocompatibility [14]. Green synthesis methods provide tunable properties for Mn_2O_3 NPs by adjusting reaction parameters or using natural reducing agents. This allows for tailored properties for specific applications like catalysis, sensors, and optoelectronics [15]. Green-synthesized metal oxide NPs often exhibit enhanced stability and functionality due to natural capping agents or biomolecules on their surfaces [16].

Metal NPs and oxides offer valuable biomedicine benefits due to their large surface area, reduced size, and light-absorbing properties. They are used for their antimicrobial, antitumor, anti-larvicidal, and antihyperglycemic properties. [17]. Mn oxides have drawn particular interest among other 3D transition metal oxides because of their numerous compositional and structural variations, including MnO, Mn_5O_8, Mn_2O_3, MnO_2, and Mn_3O_4 [18]. Their physicochemical characteristics and several applications in biosensory, catalysis, ion exchange, molecule sorption, energy storage, and drug delivery have all been investigated [19,20]. Additionally, Mn oxides often have lower toxicity levels than other compounds, which form the basis for most NPs. They are also more environmentally friendly, stable, have higher specific capacitance, and are more economical [21].

Pluronic F-127 (PF-127) is an amphiphilic triblock copolymer consisting of a central hydrophilic polyethylene oxide chain surrounded by two hydrophobic polypropylene oxide chains [22]. Due to its strong dissolving power, biocompatibility, reverse gelation, and low toxicity, PF-127 is considered an excellent medium for effective drug delivery via a variety of parenteral and non-parenteral routes [19]. Extensive research on the functional properties of these polymers in recent years has led to the development of several systems widely used as drug delivery and release mechanisms for proteins, nucleic acids, and peptides [23].

Herbal extracts contain phytochemicals such as alkaloids, polyphenols, tannins, terpenoids, and alcohol, which stabilize and reduce NPs. These plant extracts inhibit microbial pathogens and are used in green Mn_2O_3 NP synthesis [24]. Lemon, kalopanax, *Syzygium, Phyllanthus*, ananas, dittrichia, and yucca extracts are used in synthesis techniques for green Mn_2O_3 NPs [25]. However, the leaves from the plant *Glycyrrhiza uralensis* (GU) have not been employed for green Mn_2O_3 NP synthesis. A perennial herb belonging to the genus *Glycyrrhiza*, licorice is mostly found in China [26]. Licorice is widely used in various industries, including food, tobacco, cosmetics, health care, and pharmaceuticals [27]. With over 400 chemicals identified, it has strong antitussive, asthmatic, hepatoprotective, anti-inflammatory, antiviral, anti-ulcer, and anti-diabetic properties [23].

Licorice's underground component is used in China for various illnesses, while its aerial components, such as leaves, have significant nutritional content [28].

The current study describes the environmentally friendly synthesis and characterization of PF-127-encapsulated Mn_2O_3 NPs with the GU leaf extract, as well as their biomedical applications, including antimicrobial and anticancer activity against MDA-MB-231 and MCF-7 breast cancer cells.

2 Materials and methods

2.1 Materials and reagents

The cell culture media, consumables, and chemicals, including manganese(II) nitrate tetrahydrate ($Mn(NO_3)_2{\cdot}4H_2O$) and PF-127, were provided by Sigma Aldrich, USA.

2.2 Preparation of the GU leaf extract

About 10 g of fresh GU leaves were mixed with 100 mL of ethanol and boiled for 20 min at 80°C. The obtained extract was filtered using filter paper. The liquid was collected in an Erlenmeyer flask and stored at 37°C for later use.

2.3 Preparation of PF-127-encapsulated Mn_2O_3 NPs

To prepare PF-127-encapsulated Mn_2NO_3 NPs, 100 mL of the GU leaf extract was mixed with 0.1 M of manganese(II) nitrate tetrahydrate ($Mn(NO_3)_2{\cdot}4H_2O$) and 0.5 g of PF-127. The resulting green–yellow homogeneous mixture solution was continuously agitated at 80°C for 5 h. The white precipitates were allowed to dry for 1 h at 120°C. The powdered PF-127-coated Mn_2O_3 NPs were annealed at 800°C for 5 h before collection for further use.

2.4 Characterization of PF-127-coated Mn_2O_3 NPs

A Bruker-AXS D5005 X-ray diffractometer was used to characterize PF-127-coated Mn_2O_3 NPs. The Cu–K radiation with a wavelength equal to 0.1541 nm was used for the analysis, which was scanned at an angle of 2° between 20° and 90°. The average particle size of the NPs was estimated by dynamic light scattering (DLS). The experiment was carried out with NPs suspended in deionized distilled water at a scattering angle of 90° and a temperature of 25°C. The size and surface morphologies of PF-127-coated Mn_2O_3 NPs were determined by field emission scanning electron microscopy (FESEM) on a Hitachi s-4800II equipped with electron diffracted X-ray spectroscope (EDAX) to study the elemental arrangement of the formulated NPs. A photomicrograph was taken at 20 kV. To study the NP morphology further, a transmission electron microscope (TEM; Jeol Jem-2010F) was employed. In brief, the NPs were smeared on a copper grid and illuminated with electronic radiation in a vacuum. After passing through the material, an electron beam captured microphotographs. The functional groups in the PF-127-encapsulated Mn_2O_3 NPs were investigated using Fourier transform infrared (FTIR) spectroscopy (NicoletiS50). The reflectance method was used to identify the IR spectrum. The NPs were ground with KBr in a 1:100 ratio and flattened into discs to make potassium bromide (KBr) discs. The discs were scanned in the 400–4,000 cm^{-1} range directly into the spectrometer. To confirm the formation of the NPs and identify the surface plasmon resonance peak, the NPs were subjected to double-beam ultraviolet-visible (UV-Vis) spectroscopy (Shimadzu UV-2550, USA). The nanomaterials were tested in the wavelength range of 1,200–200 nm three times to determine the mean absorbance of the NPs. Photoluminescence (PL) spectroscopy (Roithner Laser Technik) was used to assess the optical properties of the NPs. The spectra were examined at exc = 470 nm using the 350–550 nm spectral area. The experiment was run three times, and the energy band gap was calculated by plotting Tauc with the following equation:

$$(h\nu\alpha)1/n = A(h\nu - E_g) \quad (1)$$

where h is Planck's constant; A is the constant proportion; α is the absorption coefficient; ν is the vibration frequency; E_g is the band gap; n is the sample transition nature [29].

2.5 Biological studies

2.5.1 Antimicrobial efficacy of PF-127-coated Mn_2O_3 NPs

PF-127-coated Mn_2O_3 NPs were tested against Gram-negative bacteria (*Klebsiella pneumoniae, Shigella dysenteriae,*

and *Escherichia coli*) and *Candida albicans* using the disc diffusion technique suggested by Elderdery et al. [30].

2.6 *In vitro* anticancer activity of PF-127-coated Mn_2O_3 NPs

2.6.1 Maintenance of cell lines

MDA-MB-231 and MCF-7 cells were provided by ATCC, which were kept in Dulbecco's modified Eagle's medium with 10% fetal bovine serum at 37°C for 5% CO_2.

2.6.2 Cytotoxicity assay

The anticancer potential of PF-127-coated Mn_2O_3 NPs was assessed using a cell viability test. MDA-MB-231 and MCF-7 cells were grown, treated with various NP concentrations (1.25, 2.5, 5, 10, 20, 40 $\mu g \cdot mL^{-1}$), and incubated for 24 h. 3-(4,5-Dimethylthiazol-2-yl)-2,5-diphenyltetrazolium bromide (MTT) treatment was applied, and formazan crystals were suspended and measured. The IC50 value of the NPs was determined using the Originpro8 program and three independent experiments were performed [30].

2.6.3 Analysis of apoptotic cells

The apoptotic efficiency of PF-127-coated Mn_2O_3 NPs against MDA-MB-231 and MCF-7 cells was examined using the dual ethidium bromide/acridine orange staining method. Cells were exposed to IC_{25} and IC_{50} NPs for 24 h, treated with an acridine orange/ethidium bromide solution for 5 min, and rinsed with phosphate-buffered saline (PBS) before being examined under an EVOS Cell Imaging System (Thermo Fisher Scientific Inc., MA, USA) [30].

2.6.4 4′,6-Diamidino-2-phenylindole (DAPI) staining

DAPI staining was used to assess nuclear DNA damage in breast cancer cells treated with PL-127-encapsulated Mn_2O_3 NPs. Cells were seeded, incubated at IC_{25} and IC_{50} concentrations, and stained with 200 $ng \cdot mL^{-1}$ DAPI fluorescent dye for 15 min. The EVOS Cell Imaging System was used to investigate nuclear damage in treated cells (Thermo Fisher Scientific Inc.).

2.6.5 JC-1 staining

Breast cancer cells were treated with green-synthesized Mn_2O_3 NPs, and their mitochondrial matrix protein (MMP) status was evaluated using JC-1 fluorescent staining. Both cells were separately cultured at a density of 2×10^5 per well in a 6-well plate for 24 h, then treated with NPs of IC_{25} and IC_{50} values. Later, 1 $\mu g \cdot mL^{-1}$ of JC-1 fluorescent dye was loaded into the wells for 20 min and then washed in PBS before being examined under a fluorescence microscope (Thermo Fisher Scientific Inc.).

2.6.6 DCFH-DA staining

Endogenous reactive oxygen species (ROS) accumulation in both treated and control breast cancer cells was measured using DCFH-DA fluorescent staining. Both cells were cultured in a 24-well plate for 24 h before being administered with NPs of IC_{25} and IC_{50} values for 24 h. The fluorescent stain DCFH-DA was then applied to each well for 1 h. The level of endogenous ROS was then measured in both control and treated cells using a fluorescent microscope (Thermo Fisher Scientific Inc., MA, USA).

2.6.7 Analysis of apoptosis by flow cytometry

The effect of green-synthesized Mn_2O_3 NPs on apoptosis in breast cancer cells was studied with flow cytometry. On a 6-well plate, both cells were cultured separately for 24 h. They were then exposed for 24 h to the IC_{25} and IC_{50} values of green-synthesized Mn_2O_3 NPs. Apoptosis was measured in control and treated cells by the Annexin V-FITC/PI-Apoptosis Detection Kit. After the cells were harvested, they were studied using flow cytometry according to the manufacturer's instructions (Abcam, USA).

2.6.8 Cell cycle analysis

Cells were rinsed with a buffered solution before being treated with ethanol for 12 h. The cells were then stained for 30 min with 300 µL of a staining solution containing 100 L of propidium iodide (PI), 0.08 $mg \cdot mL^{-1}$ of a proteinase inhibitor, and 0.5 $mg \cdot mL^{-1}$ of RNase. Flow cytometry was used to measure PI fluorescence in relation to DNA. The MultiCycle program (Phoenix Flow Systems, USA) was used to examine nuclei percentages at various stages of the cell cycle.

2.7 Statistical analysis

All experiments were run in triplicate, and the data were statistically analyzed using a one-way ANOVA and a posthoc Tukey post-test. The values are presented as mean ± standard deviation, with statistical significance set at $P < 0.05$.

3 Results

3.1 Characterization of green PF-127 Mn_2O_3 NPs

3.1.1 UV-Vis spectrometry analysis

The optical properties of PL127-coated Mn_2O_3 NPs were investigated using a UV-visible (UV-Vis) spectrometer, and UV-Vis wavelengths ranging from 200 to 1,100 nm were recorded. The UV and optical spectrum of PL-127-encapsulated Mn_2O_3 NPs is depicted in Figure 1a. When electrons are excited from the filled to the empty band, Mn_2O_3 NPs' absorbance edges are visible at 232 and 394 nm (Figure 1a) [31].

3.1.2 FTIR spectrum analysis

The functional groups present in GU were identified and their function in the synthesis of PL127-coated Mn_2O_3 NPs was investigated. The findings of the FTIR study show that the surface of the NPs contains components like alkaloids, glycosides, and tannins. In the process of reducing Mn ions and stabilizing PL127-coated Mn_2O_3 NPs, FTIR measurements were employed to ascertain how manganese salts and protein molecules interacted. At 3,419 cm^{-1}, the strong O–H stretching peaks could be observed. Peaks in the PF127 functional group for the C–H asymmetric stretching, C–H symmetric stretching, O–H bending, and C–O–C stretching were all detected at 2,924, 2,854, 1,384, and 1,082 cm^{-1},

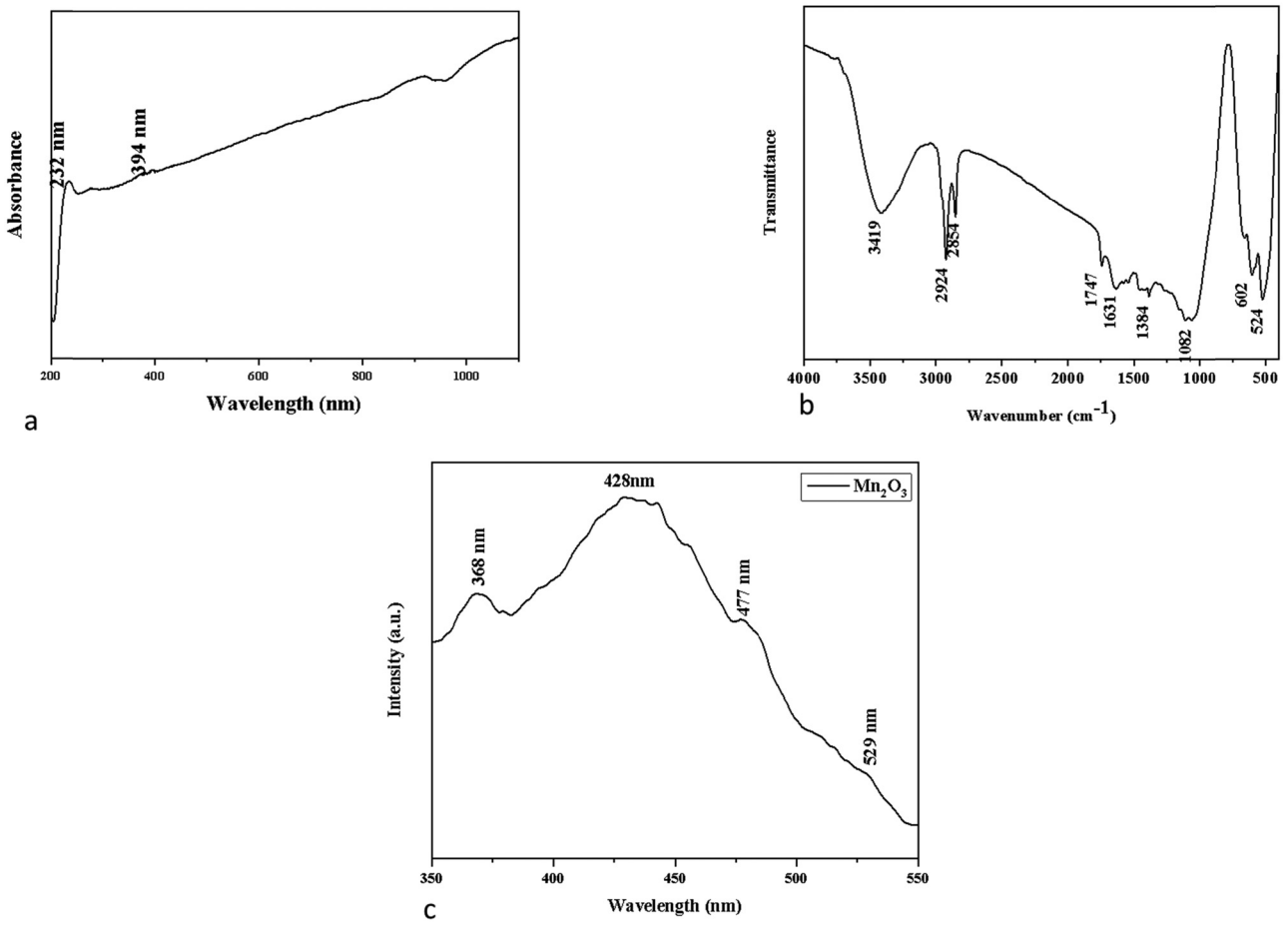

Figure 1: UV-Vis spectrophotometer: (a) FTIR transmittance vs wavenumber chart, (b) PL spectrum, (c) and analysis of synthesized PF-127-coated Mn_2O_3 NPs.

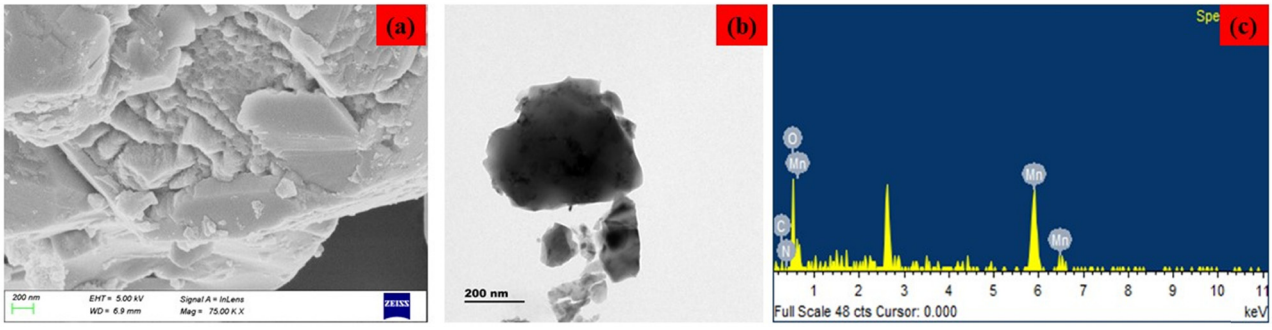

Figure 2: (a and b) FESEM and TEM images and (c) EDAX spectrum of Mn_2O_3 NPs.

respectively. At 1,631 cm^{-1}, the C–O–H stretching and O–H bending vibration bands were detected. Two significant peaks at 602 and 524 cm^{-1} were produced by the stretching vibrations of the Mn–O and Mn–O–Mn bonds, as illustrated in Figure 1b [32]. The outcomes demonstrate the presence of hydroxyl and carboxyl groups on the surface of PL127-coated Mn_2O_3 NPs.

3.1.3 PL spectroscopy

Figure 1c displays the PL emission spectra of PL127-coated Mn_2O_3 NPs with an excitation wavelength of 325 nm that were obtained at room temperature. The figure illustrates that the PL spectra of PL127-coated Mn_2O_3 NPs have several peaks in the UV and visible regions. The near-band emissions, which mostly originate from the recombination of the free excitons through an exciton–exciton collision mechanism, are the principal components of the UV emission, which has a single strong and broad-centered peak at around 368 nm [33]. Additionally, there are three peaks in the visible emission spectrum at about 428, 477, and 529 nm. Given the fact that oxygen vacancies and intrinsic defects are intensely confined, all visible emission bands can be attributed to defects [34].

3.1.4 Morphology and chemical composition

Figure 2a and b displays an FESEM/TEM imaging of green PL127-coated Mn_2O_3 NPs. In TEM images, the PF-127-encapsulated Mn_2O_3 NPs can be observed to have a nanoflake-like structure. Particles were shown to range in size from 120 to 150 nm. An EDAX spectrum was used to examine the chemical composition of the PF-127-encapsulated Mn_2O_3 NPs, as shown in Figure 2c. The NPs contain the following atomic percentages: 12.261% C, 4.86% N, 42.61% Mn, and 40.27% O.

3.1.5 X-ray diffraction (XRD) analysis

Figure 3a displays the XRD diffraction spectra for Mn_2O_3 NPs. The planes (211), (222), (400), (332), (413), (440), and

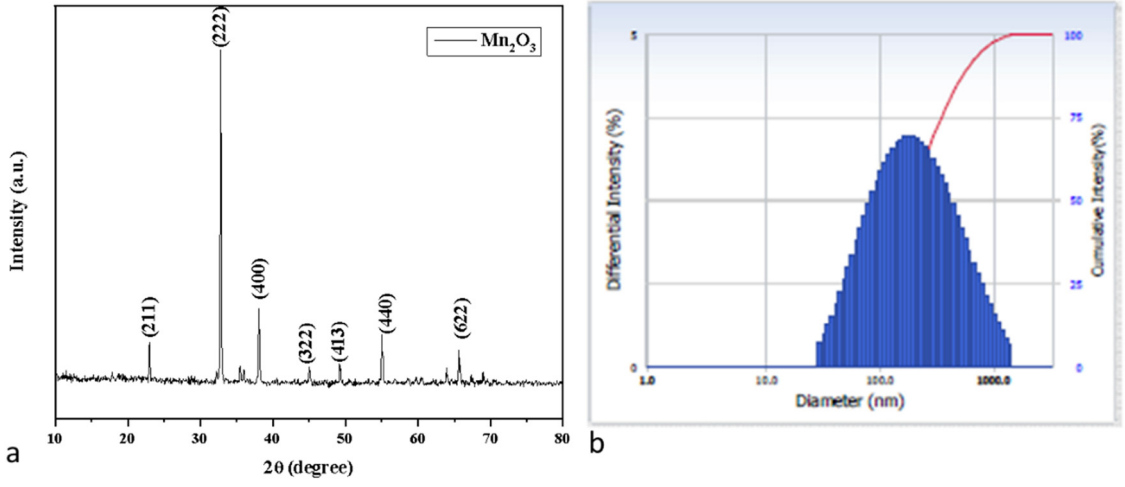

Figure 3: XRD pattern of PF-127-coated Mn_2O_3 NPs (a) and DLS spectrum of Mn_2O_3 NPs (b).

(622) of Mn_2O_3 NPs are represented by the peaks at 22.8°, 32.7°, 37.99°, 44.96°, 49.12°, and 55.02°, respectively, in the XRD spectrum. The *hkl* planes are well-indexed to a cubic structure in comparison to the typical peaks of pure Mn_2O_3 (JCPDS 41-1442) [35]:

$$\text{Average crystallite size}(D) = \frac{0.9\lambda}{\beta\cos\theta} \quad (2)$$

where the X-ray wavelength (1.5406), Bragg's diffraction angle, and the angular peak width at half maximum (rad) are all given.

Green PL-127-coated Mn_2O_3 NPs have an average particle size of 80 nm. Following a successful synthesis, the average particle size of the NPs was estimated using the Debye–Scherrer equation and an examination of the material's crystallinity [36].

3.1.6 DLS study

The hydrodynamic size of PL127-coated Mn_2O_3 NPs was calculated using DLS to determine the particle size, as

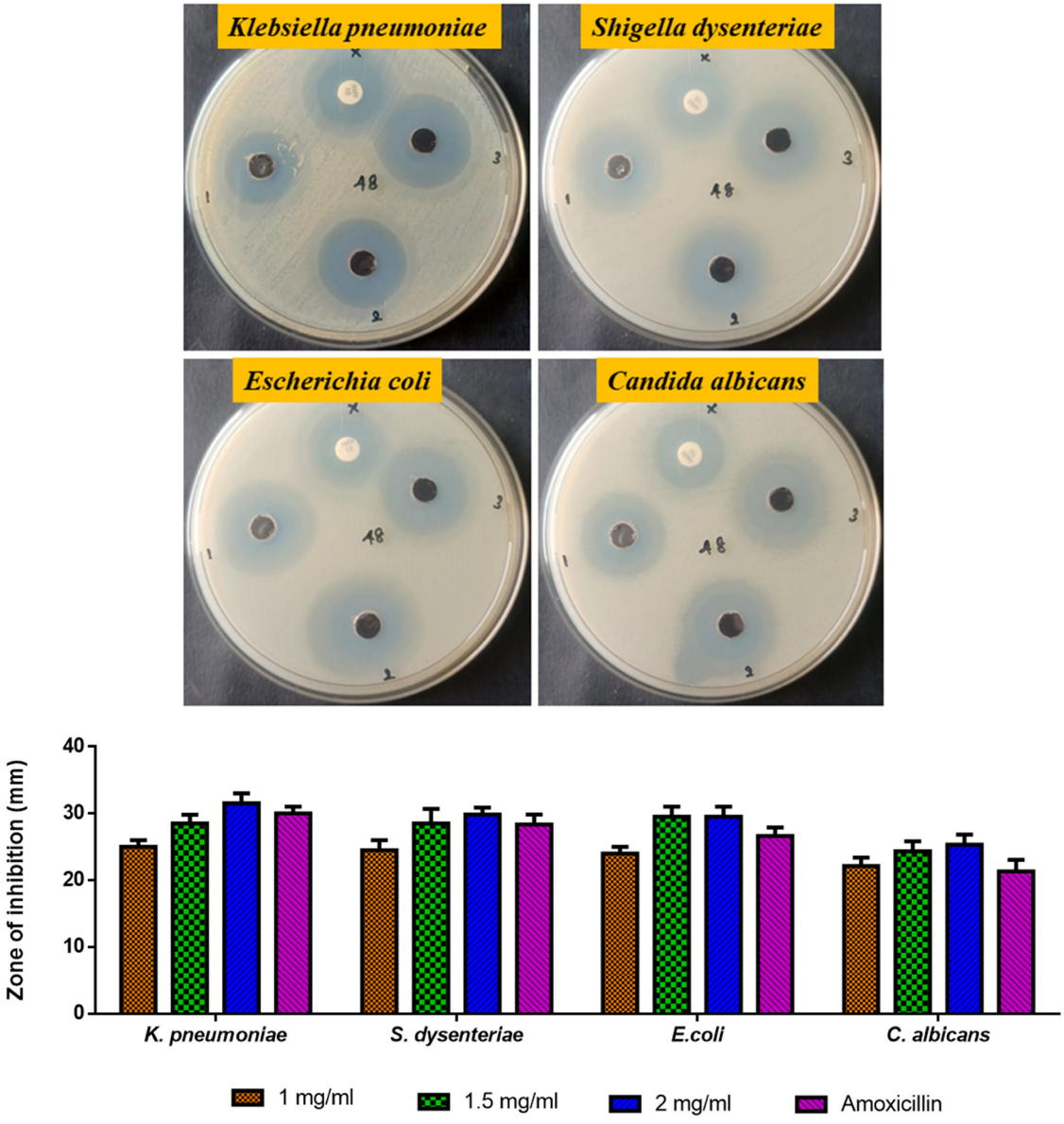

Figure 4: Antibacterial activity of PF-127-coated Mn_2O_3 NPs. NPs inhibit the growth of bacteria and fungi. Antibacterial activity was determined for PF-127-coated Mn_2O_3 NPs by measuring the zone of inhibition.

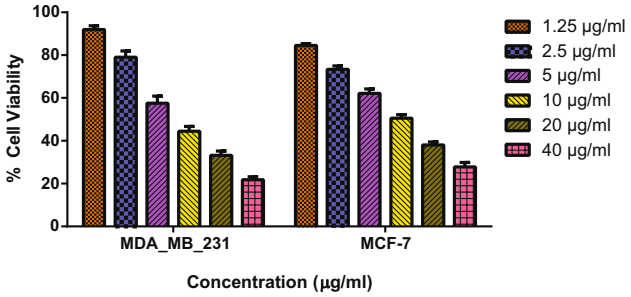

Figure 5: PF-127-coated Mn_2O_3 NPs cause cytotoxicity in MDA-MB-231 and MCF-7 cells. MDA-MB-231 and MCF-7 cell lines were treated with different concentrations (1.25–40 µg·mL^{-1}) of PF-127-coated Mn_2O_3 NPs for 24 h. The cells were subjected to MTT assay, and the values were depicted as ± SD of three individual experiments.

shown in Figure 3b. Because a water medium encircled the PL127-coated Mn_2O_3 NPs, which were measured at 195.50 nm in size, the DLS particle size was larger than that of the XRD results. This sizing is known as the hydrodynamic size.

3.2 Antimicrobial activity of Mn_2O_3 NPs

The antibacterial activity of PL127-coated Mn_2O_3 NPs was assessed against Gram-negative bacterial strains (*K. pneumonia*, *S. dysenteriae*, and *E. coli*) and the fungus *C. albicans*, as depicted in Figure 4a. Amoxicillin, an antibiotic, and green PL127-coated Mn_2O_3 both exhibited substantial antimicrobial properties. In comparison to amoxicillin, the PL127-coated Mn_2O_3 NPs demonstrated larger zones of inhibition (Figure 4b). Additionally, the antimicrobial activity improved as the nanoparticle concentration increased.

3.3 Anticancer activity

3.3.1 Cytotoxicity analysis by MTT assay

The biosynthesized PL127-coated Mn_2O_3 NPs were examined for their cytotoxicity by MTT assay against MDA-MB-231 and MCF-7 cells at various dosages (1.25, 2.5, 5, 10, 20, 40 µg·mL^{-1}) for 24 h. The NPs exhibited significant cytotoxic effect against MDA-MB-231 (IC_{50} = 8 µg·mL^{-1}) and MCF-7 (IC_{50} = 10 µg·mL^{-1}) cells at 24 h (Figure 5). Moreover, the cell viability was observed to decrease with increasing NP dose.

3.3.2 Apoptotic cell death analysis

Both cells were stained with AO/EB dyes and two doses of green PL127-coated Mn_2O_3 NPs (IC_{25}, IC_{50}), and were then examined under a fluorescence microscope. The control

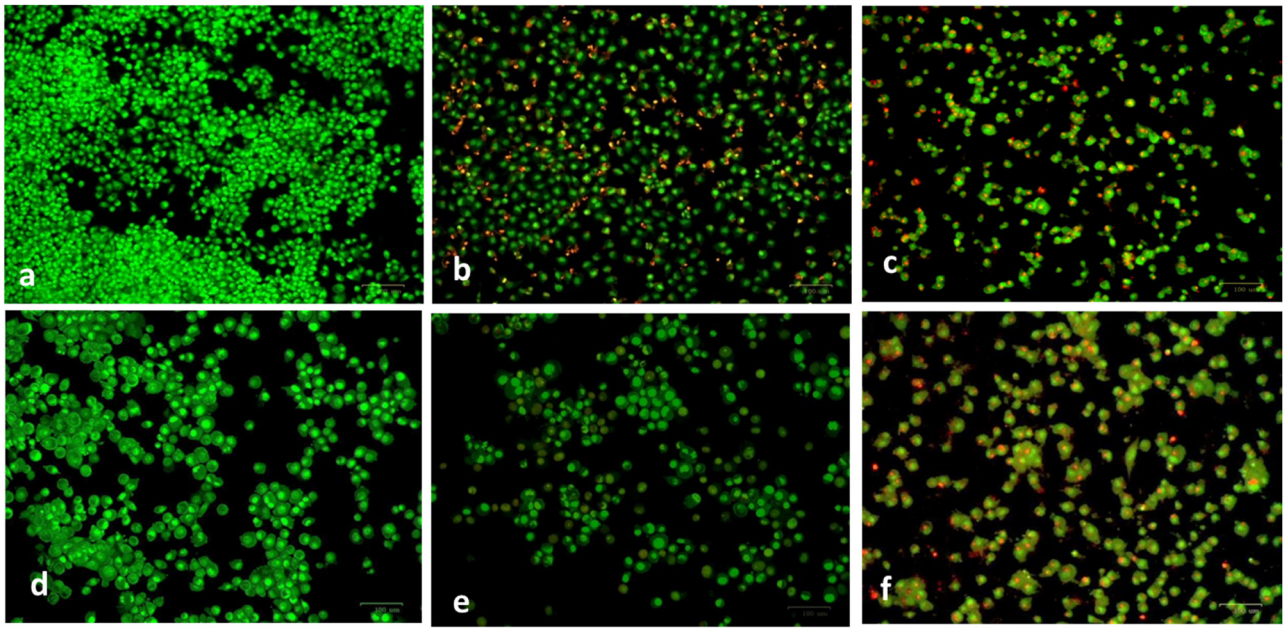

Figure 6: Apoptosis was determined in MDA-MB-231 and MCF-7 cells by using AO/EtBr dual staining with IC_{25} and IC_{50} doses of PF-127-coated Mn_2O_3 NPs after 24 h of treatment. MDA-MB-231: control cells (a), cells treated with IC_{25} (b), and IC_{50} (c) of PF-127-coated Mn_2O_3 NPs. MCF-7: control cells (d), cells treated with IC_{25} (e), and IC_{50} (f) of PF-127-coated Mn_2O_3 NPs. This is a representative image of the experiment performed in triplicate at a magnification of 20×.

cells showed green fluorescence, indicating that they were not apoptotic. PlF-127-coated Mn_2O_3 NP-treated cells showed yellow/orange fluorescence, indicating early and late apoptosis with condensed nuclei (Figure 6).

3.3.3 Analysis of apoptotic nuclear changes by DAPI staining

DAPI staining was used to analyze the apoptosis in the control and treated breast cancer cells. As demonstrated in Figure 7, the control cells exhibited fewer fluorescent cells, which indicates viable cells without or with less apoptosis. However, both cells exposed to (IC_{25}, IC_{50}) green-synthesized PL127-coated Mn_2O_3 NPs demonstrated increased blue fluorescence, indicating the occurrence of higher apoptotic cell death with increased structural damages, nuclear injury, and apoptotic body formations in both cells (Figure 7b and c).

3.3.4 MMP analysis

The PL127-loaded Mn_2O_3 NP-induced changes in breast cancer cells' MMP were examined by JC-1 staining, and the results are shown in Figure 8. The untreated control cells exhibited red fluorescence, which reveals intact MMP. However, both cells, which were exposed to the (IC_{25}, IC_{50}) green-synthesized PL127-coated Mn_2O_3 NPs, produced increased green fluorescence, which indicates that PL127-coated Mn_2O_3 NP treatment could reduce MMP levels of breast cancer cells (Figure 8).

3.3.5 Analysis of ROS accumulation

The role of ROS generation in green-synthesized PL127-coated Mn_2O_3 NPs-induced apoptosis in breast cancer cells is of utmost importance. Figure 9 depicts the effect of green-synthesized PL127-coated Mn_2O_3 NPs on endogenous ROS accumulation in breast cancer cells. As displayed in Figure 9, the control cells exhibited poor green fluorescence, which reveals less ROS generation; whereas, the MDA-MB-231 and MCF-7 cells, which were exposed to (IC_{25}, IC_{50}) green-synthesized PL127-coated Mn_2O_3 NPs, demonstrated increased green fluorescence, which reveals increased ROS levels.

3.3.6 Analysis of apoptosis by flow cytometry

In the current study, the Annexin V/PI assay, which assesses apoptosis, was utilized to further study the potential cell death mechanisms of the breast cancer cells following treatment with the green-synthesized PL127-coated Mn_2O_3 NPs. The percentage of apoptotic cells in treated breast cancer cells was investigated using flow cytometry analysis (Figure 10). The results of flow cytometry indicated that treatments with (IC_{25}, IC_{50}) green-synthesized

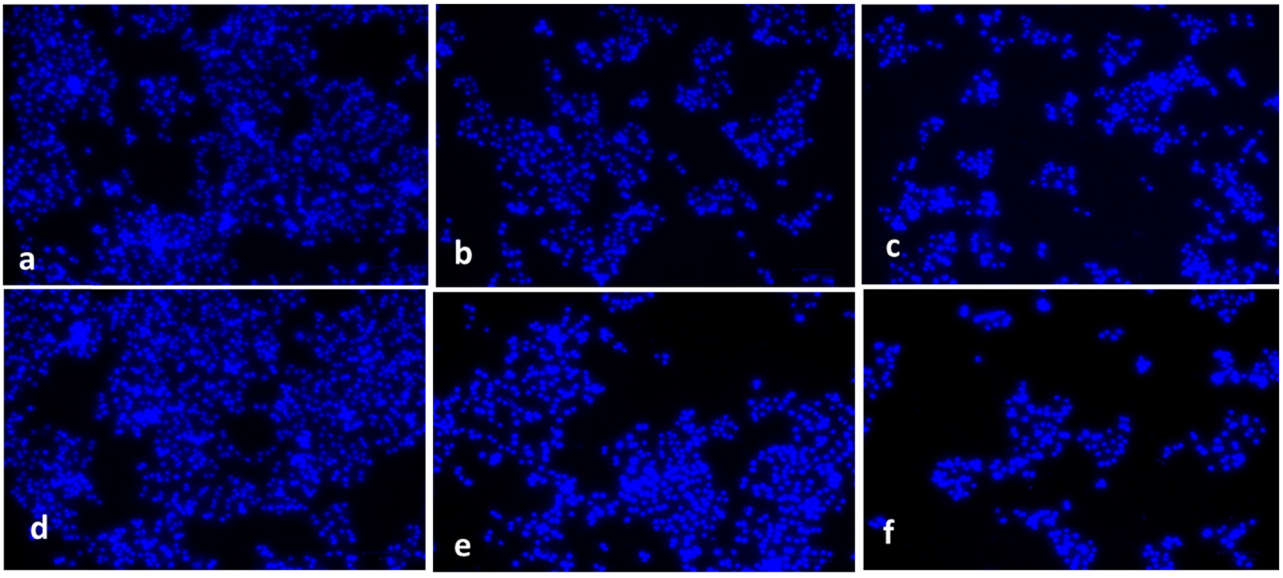

Figure 7: DAPI nuclear staining was used to determine apoptosis in MDA-MB-231 and MCF-7 cells. MDA-MB-231: control cells (a), cells treated with IC_{25} (b), and IC_{50} (c) of PF-127-coated Mn_2O_3 NPs; MCF-7: control cells (d), cells treated with IC_{25} (e), and IC_{50} (f) of PF-127-coated Mn_2O_3 NPs. This is a representative image of the experiment performed in triplicate at a magnification of 20×.

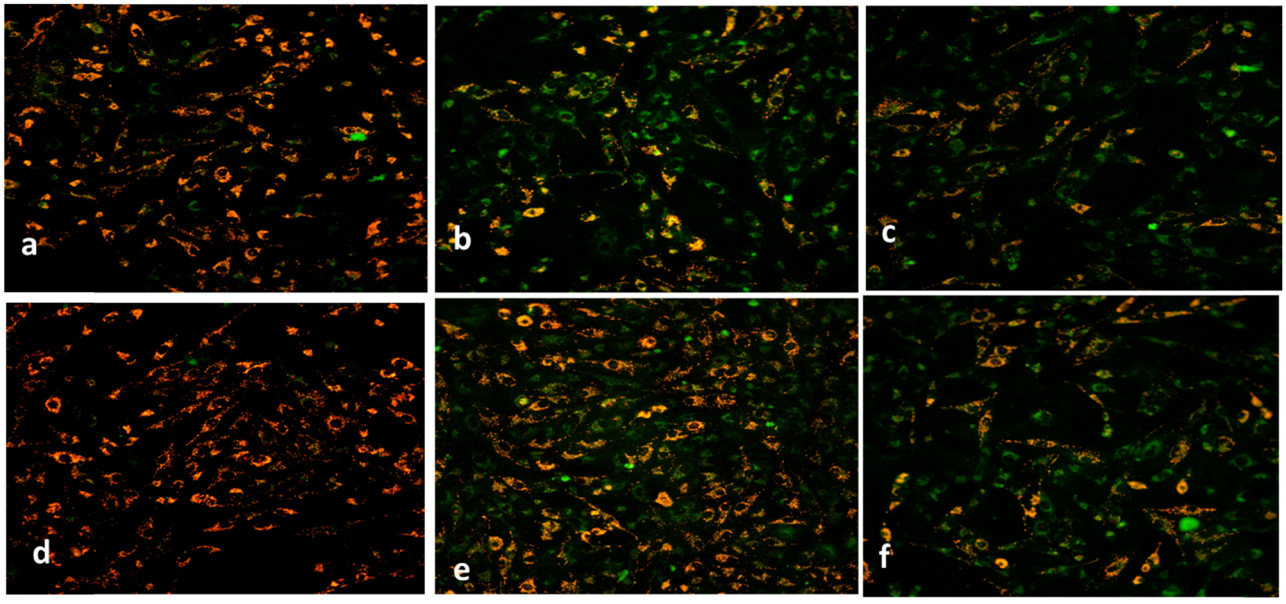

Figure 8: In MDA-MB-231 and MCF-7 cells treated for 24 h with PF-127-coated Mn_2O_3 NPs, the mitochondrial membrane potential was determined by JC-1 staining. MDA-MB-231: control cells (a), cells treated with IC_{25} (b), and IC_{50} (c); MCF-7: control cells (d), cells treated with IC_{25} (e), and IC_{50} (f). This is a representative image of the experiment performed in triplicate at a magnification of 20×.

PL127-coated Mn_2O_3 NPs considerably augmented the apoptotic cell proportions in both cells. Both cells showed higher apoptosis after treatment with PL127-coated Mn_2O_3 NPs (Figure 10).

3.3.7 Cell cycle analysis

Flow cytometry was used to detect cell cycle inhibition in control and treated breast cancer cells (Figure 11). Following

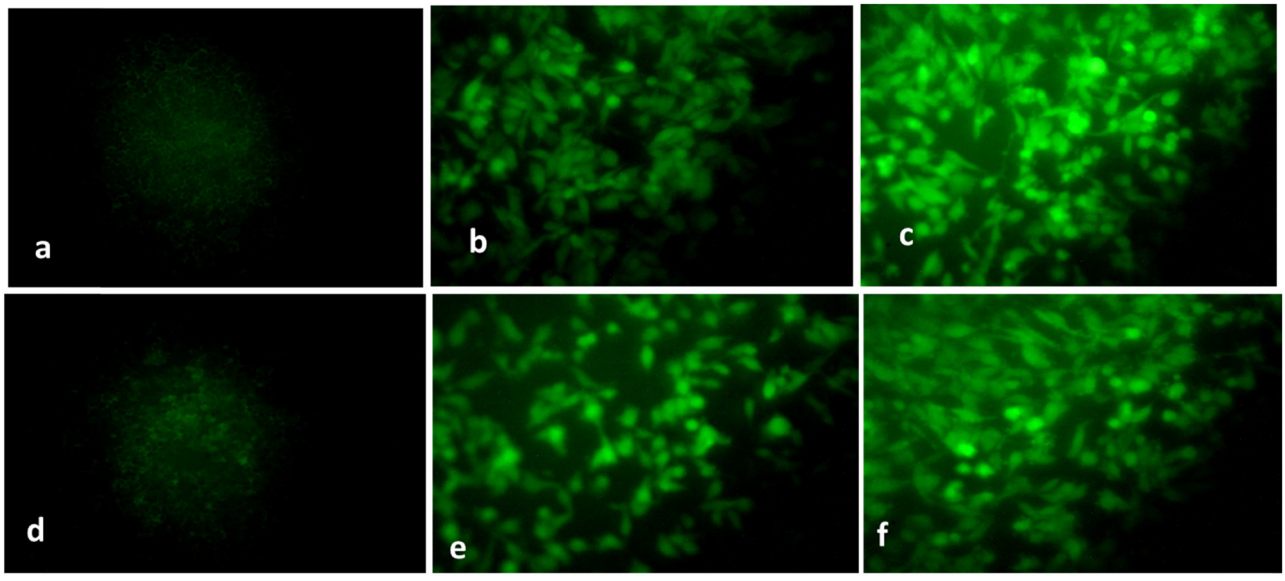

Figure 9: A fluorescence microscope image stained with DCF-DA. MDA-MB-231: control cells (a), cells treated with IC_{25} (b), and IC_{50} (c) of PF-127-coated Mn_2O_3 NPs; MCF-7: control cells (d), cells treated with IC_{25} (e), and IC_{50} (f) of PF-127-coated Mn_2O_3 NPs. This is a representative image of the experiment performed in triplicate at a magnification of 20×.

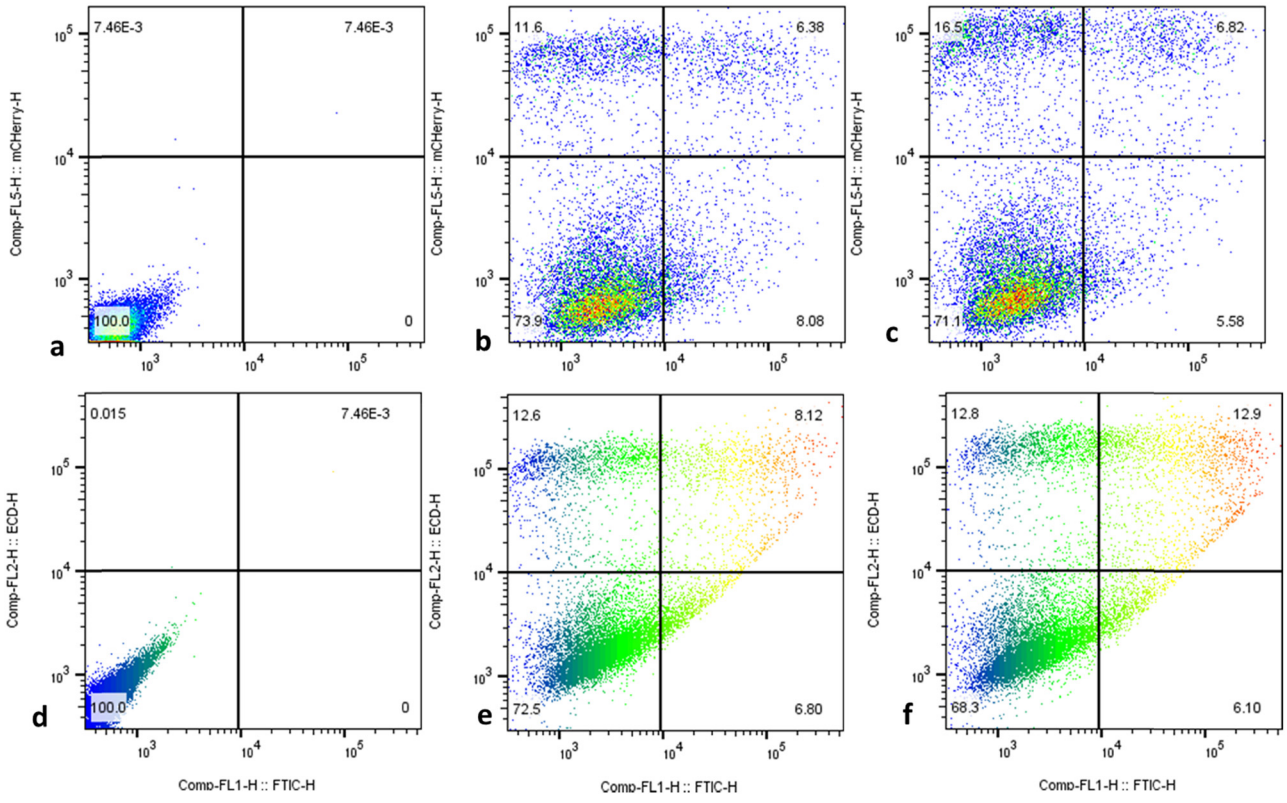

Figure 10: Annexin-V/-FITC/PI Flow cytometry analysis of MDA-MB-231 and MCF-7 cancer cells treated with IC_{50} concentration of PF-127-coated Mn_2O_3 NPs for 24 h. These figures are from representative experiments carried out in at least two independent tests. MDA-MB-231: control cells (a), cells treated with IC_{25} (b), and IC_{50} (c); MCF-7: control cells (d) cells treated with IC_{25} (e), and IC_{50} (f). Data were mean ± SD of two independent experiments. *$p < 0.05$ when compared with control, **$p < 0.001$ when compared with control.

treatment with green-synthesized PL127-coated Mn_2O_3 NPs, both cells showed an increase in the S-phase cell proportion. Furthermore, after exposure to Mn_2O_3 NPs, cell proportions in the G1 phase were significantly reduced in both cells. These results show that treatment with PL127-coated Mn_2O_3 NPs induces cell cycle arrest in the S phase in breast cancer cells (Figure 11).

4 Discussion

Cancer, one of the most debilitating illnesses in the world, leads to the death of millions of individuals in underdeveloped nations. It has been documented that oxidative stress is a crucial factor in the emergence and progression of multiple diseases that affect essential organs, especially cancer [37]. Breast cancer ranks among the most often diagnosed types of cancer. Breast cancer can be treated with several treatment methods, including surgery, radiation therapy, and chemotherapy. Unfortunately, these treatments can have negative impacts on healthy cells [38]. The existing chemotherapeutic drugs have a very constrained therapeutic range, limited solubility, and are hazardous to healthy tissues [39]. In this aspect, polymer-based drug delivery systems can provide highly localized drug concentration in tumorous regions with no detrimental impact on healthy cells [40].

The antimicrobial mechanism of NPs can be ascribed to an electrochemical action model that permeates and damages the cell walls of the microbes, thereby inhibiting their growth [41]. The remarkable antimicrobial activity of Mn_2O_3 NPs is attributable to electron transport in an oxidized and reduced state, and NPs are believed to have inactivated bacterial enzymes, producing H_2O_2 and resulting in bacterial cell death [42]. Moreover, their physical properties including size and morphology in addition to the functionalization with the plant extract molecules are also equally responsible for the high antimicrobial effect displayed by NPs. The findings demonstrate that Mn_2O_3 NPs have outstanding antimicrobial characteristics and have the potential to provide effective targeted delivery to the microbes for maximized bactericidal effect [43]. Factors influencing the biological activity of inorganic NPs include size distribution, morphology, surface charge,

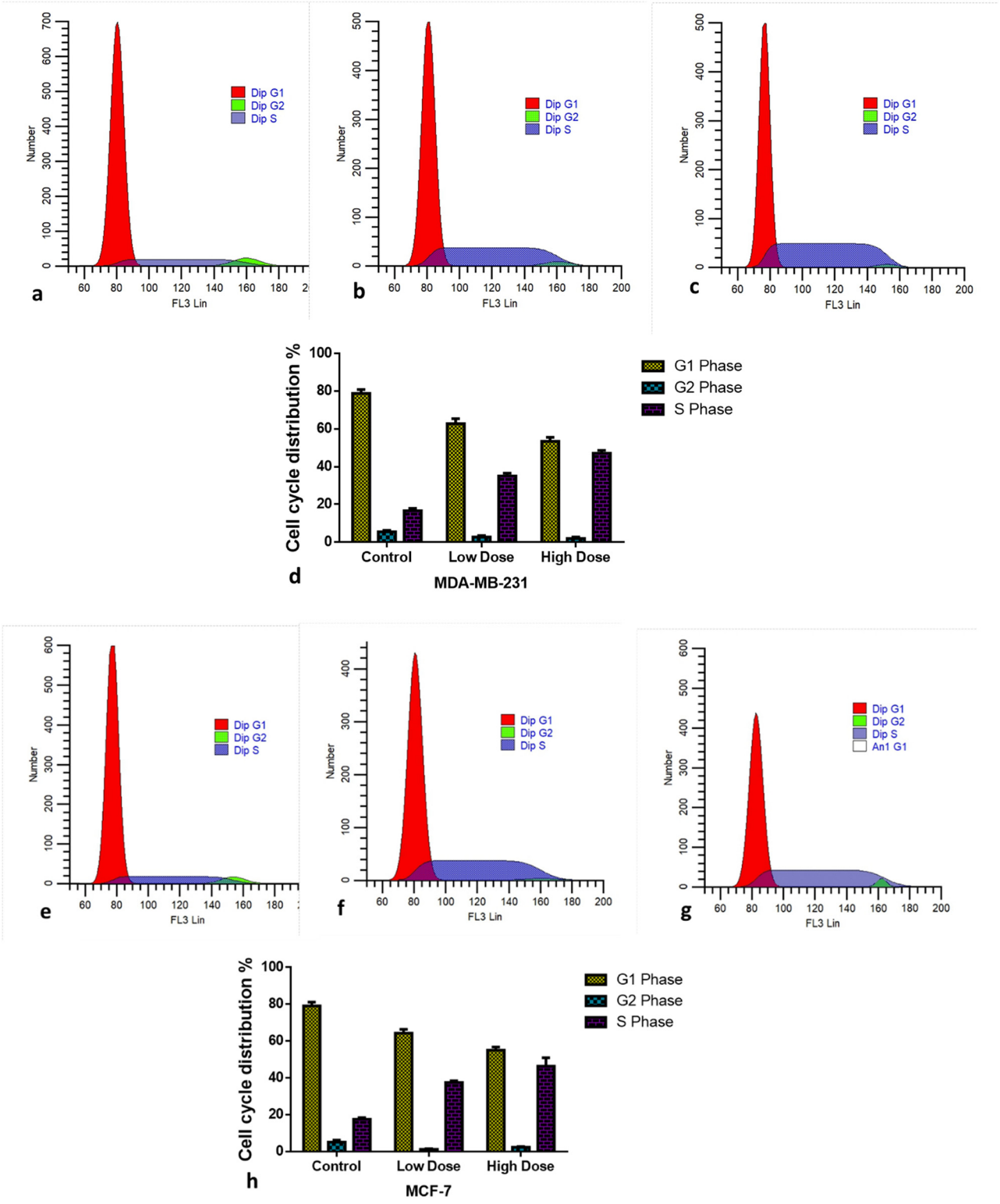

Figure 11: Cell cycle analysis using flow cytometry after staining with PI. MDA-MB-231 and MCF-7 cells were treated with IC_{25} and IC_{50} concentrations of PF-127-coated Mn_2O_3 NPs for 24 h. Cell cycle pattern and apoptosis distribution in MDA-MB-231: control cells (a), treated with IC_{25} (b) and IC_{50} (c), and percentage of cells distribution (d); MCF-7: control cells (e), treated with IC_{25} (f) and IC_{50} (g), and percentage of cells distribution (h).

surface chemistry, and capping agents. These variables can improve targeting efficiency, safety, and effectiveness in biomedical applications like drug delivery, imaging, diagnostics, and therapy [44].

The MTT technique, which relies on the formation of formazan complex via the reduction of MTT or other tetrazolium salts, is a cytotoxicity assay to assess the cell death rate. Numerous studies have demonstrated that the elimination of free radicals promotes the anti-cancer activity exerted by metallic NPs [45]. Oxidative stress induced by elevated ROS levels inside the cells ultimately results in programmed cell death. Additionally, damaged mitochondrial membranes caused by high ROS levels have been associated with cell death. Additionally, PF-127 that was utilized to encapsulate the NPs has been demonstrated to interact with cancerous cells, thereby chemo-sensitizing them [46].

Green NPs cause cell death through loss of membrane integrity due to the release of Mn^{4+} ions, which trigger ROS accumulation. This further enhances DNA damage, mitochondrial dysfunction, and apoptotic cell death due to ROS-induced oxidative stress [47]. The initiating factors and hallmarks of apoptosis are shrinkage and detachment of cells, plasma membrane protrusions, and the development of apoptotic bodies and nuclear fragmentations. Quercetin-loaded AuNPs effectively induce higher apoptotic incidences in breast cancer cells, supporting the ability of green-synthesized Mn_2O_3 NPs to induce apoptosis [48]. Anticancer drugs activate apoptosis via the mitochondrial pathway, with altered MMP, which is a key indicator of apoptosis [49,50]. The treatment with MnO_2 NPs led to decreased MMP levels in breast cancer MCF-7 cells, consistent with the current findings [51].

ROS have long been linked to tumor growth due to their influence on cellular proliferation and chemotherapy resistance. Cellular damage or death, on the other hand, can result from either an excess of ROS accumulation or a compromised cell's ability to counteract ROS. As a result of oxidative stress, tumor cells die due to their excessive ROS accumulation [52]. Overproduction of ROS is a common effect of chemotherapeutic drugs that might initiate apoptosis. These findings evidence that treatment with Mn_2O_3 NPs induces oxidative stress in breast cancer cells by increasing ROS. This study's findings were supported by a previous study demonstrating increased ROS accumulation in MDA-MB-231 and MCF-7 cells after carbon nanoparticle treatment [53].

Previously, MnO_2 NPs were synthesized from the *Saraca asoca* leaf extract (SA-MnO_2 NPs), which were found to be significantly cytotoxic against MDA-MB-231 and MCF-7 cells [54]. Based on an evaluation of green-derived MnO_2 NPs using *Viola betonicifolia* leaf extract against MCF-7 breast cancer cells, up to 96% inhibition was observed in earlier studies [55]. A study found that green-fabricated MnO_2 NPs derived from the *Terminalia chebula* fruit extract inhibited MCF-7 breast cancer cells [56]. In earlier studies, green MnO_2 NPs prepared using the *Gmelina arborea* extract showed higher antitumor activity. Further, cells treated with GAE-coated MnO_2 NPs showed normalized cellular morphology, indicating improvement in antitumor activity [57]. In comparison with previous studies, our results described that the GU leaf extracts were used to synthesize Mn_2O_3 NPs that were highly cytotoxic to MDA-MB-231 and MCF-7 cells. In addition to increased ROS accumulations and decreased MMP levels, DAPI, dual staining, and flow cytometry demonstrated increased apoptosis and cell cycle inhibition.

Apoptosis, a critical component in the regulation of cell death, plays a major role in determining cancer cell growth and death. The avoidance of apoptosis is a crucial factor in tumor growth and the emergence of resistance to therapies. It had already been shown that suppressing apoptosis enhances cancer progression [58]. The flaws in apoptotic mechanisms trigger cells to proliferate continuously, which is a hallmark of tumors, and tumors are often generated by colonies of immortal cells that have mutated to evade apoptosis. Thus, inducing cancer cells to self-destruct via apoptosis is considered a promising strategy for tumor eradication. An earlier study done by Moghaddam et al. [59] highlighted that Mn_2O_3 NPs effectively induced apoptosis cell death in MCF-7 cells, which supports the current findings. The cell cycle consists of interphases (G1, S, and G2) and mitosis (M). In the G1 phase, cells grow and make RNA and proteins for DNA synthesis [60]. In the S phase, DNA replicates, and the G2 phase involves protein synthesis. The M phase divides the nucleus and cytoplasm. Controlling the tumor cell cycle is crucial for anticancer therapies. A study using green-synthesized silver NPs supports the findings [61].

5 Conclusions

Eco-friendly P127-coated Mn_2O_3 NPs coated with the GU leaf extracts have been synthesized and characterized for their antimicrobial and anticancer activities. The NPs have an average crystallite size of 80 nm and exhibit high antimicrobial efficacy against various bacterial strains and the fungal *Candida albicans*. The green-formulated PL-127-coated Mn_2O_3 NPs exhibited a significant cytotoxic effect on breast cancer cells. Increased ROS levels and reduced MMP levels were observed in PL-127-coated Mn_2O_3 NP-treated breast cancer cells. The findings of dual staining,

DAPI and Annexin V-FITC/PI staining, revealed increased apoptosis in breast cancer cells after treatment with green-synthesized PL-127-coated Mn_2O_3 NPs. Furthermore, flow cytometry analysis revealed cell cycle inhibition in breast cancer cells. Thus, it was evident that green-synthesized PL-127-coated Mn_2O_3 NPs possess significant antimicrobial and anticancer treatment options for breast cancer. Future studies will concentrate on using newly created PL-127-coated Mn_2O_3 NPs for nanodrug delivery platform design and development.

Acknowledgment: The authors extend their appreciation to the Deputyship for Research and Innovation, Ministry of Education in Saudi Arabia for funding this research work through project no. 223202.

Funding information: This research was funded by Deputyship for Research and Innovation, Ministry of Education in Saudi Arabia (project no. 223202).

Author contributions: Abozer Y. Elderdery, Badr Alzahrani: conceptualization, investigation, formal analysis, visualization, writing-original draft; Abdullah Alsrhani, Nasser A. N. Alzerwi: funding acquisition, project administration, resources; Maryam Musleh Althobiti, Ahmed M. E. Elkhalifa: conceptualization, project administration, resources, supervision, writing – review and editing; Musaed Rayzah, Bandar Idrees: investigation, formal analysis, validation, methodology; Suresh S. Kumar, Pooi Ling Mok: methodology, investigation, formal analysis, project administration, supervision, validation, visualization, writing – review and editing.

Conflict of interest: The authors state no conflict of interest.

Data availability statement: The manuscript includes all data generated during this study.

References

[1] Subhan MA, Choudhury KP, Neogi N. Advances with molecular nanomaterials in industrial manufacturing applications. Nanomanufacturing. 2021;1(2):75–97. doi: 10.3390/nanomanufacturing1020008.

[2] Nam NH, Luong NH. Nanoparticles: Synthesis and applications. Mater Biomed Eng. 2019;211–40. doi: 10.1016/B978-0-08-102814-8.00008-1.

[3] Alqarni LS, Alghamdi MD, Alshahrani AA, Nassar AM. Green nanotechnology: Recent research on bioresource-based nanoparticle synthesis and applications. J Chem. 2022;2022:4030999. doi: 10.1155/2022/4030999.

[4] Quester K, Avalos-Borja M, Castro-Longoria E. Biosynthesis and microscopic study of metallic nanoparticles. Micron. 2013;54:1–27. doi: 10.1016/j.micron.2013.07.003.

[5] Jayandran M, Haneefa MM, Balasubramanian V. Green synthesis and characterization of Manganese nanoparticles using natural plant extracts and its evaluation of antimicrobial activity. J Appl Pharm Sci. 2015;5(12):105–10. doi: 10.7324/JAPS.2015.501218.

[6] Sharma D, Kanchi S, Bisetty K. Biogenic synthesis of nanoparticles: A review. Arab J Chem. 2019;12(8):3576–600. doi: 10.1016/j.arabjc.2015.11.002.

[7] Khan SH. Green Nanotechnology for the Environment and Sustainable Development. In: Naushad M, Lichtfouse E, editors. Green materials for wastewater treatment. Environmental chemistry for a sustainable world. Vol. 38. Cham: Springer; 2020. doi: 10.1007/978-3-030-17724-9_2.

[8] Yaqoob AA, Ahmad H, Parveen T, Ahmad A, Oves M, Ismail IMI, et al. Recent advances in metal decorated nanomaterials and their various biological applications: A review. Front Chem. 2020 May 19;8:341. doi: 10.3389/fchem.2020.00341. PMID: 32509720; PMCID: PMC7248377.

[9] Yetisgin AA, Cetinel S, Zuvin M, Kosar A, Kutlu O. Therapeutic nanoparticles and their targeted delivery applications. Molecules. 2020 May;25(9):2193. doi: 10.3390/molecules25092193. PMID: 32397080; PMCID: PMC7248934.

[10] Sim S, Wong NK. Nanotechnology and its use in imaging and drug delivery (Review). Biomed Rep. 2021 May;14(5):42. doi: 10.3892/br.2021.1418. Epub 2021 Mar 5 PMID: 33728048; PMCID: PMC7953199.

[11] Kharissova OV, Kharisov BI, Oliva González CM, Méndez YP, López I. Greener synthesis of chemical compounds and materials. R Soc Open Sci. 2019 Nov;6(11):191378. doi: 10.1098/rsos.191378. PMID: 31827868; PMCID: PMC6894553.

[12] Iravani S, Korbekandi H, Mirmohammadi SV, Zolfaghari B. Synthesis of silver nanoparticles: chemical, physical and biological methods. Res Pharm Sci. 2014 Nov-Dec;9(6):385–406. PMID: 26339255; PMCID: PMC4326978.

[13] Madani M, Hosny S, Alshangiti DM, Nady N, Alkhursani SA, Alkhaldi H, et al. Green synthesis of nanoparticles for varied applications: Green renewable resources and energy-efficient synthetic routes. Nanotechnol Rev. 2022;11(1):731–59. doi: 10.1515/ntrev-2022-0034.

[14] Dikshit PK, Kumar J, Das AK, Sadhu S, Sharma S, Singh S, et al. Green synthesis of metallic nanoparticles: Applications and limitations. Catalysts. 2021;11(8):902. doi: 10.3390/catal11080902.

[15] Samuel MS, Ravikumar M, John JA, Selvarajan E, Patel H, Chander PS, et al. A review on green synthesis of nanoparticles and their diverse biomedical and environmental applications. Catalysts. 2022;12(5):459. doi: 10.3390/catal12050459.

[16] Shafey AME. Green synthesis of metal and metal oxide nanoparticles from plant leaf extracts and their applications: A review. Green Process Synth. 2020;9(1):304–39. doi: 10.1515/gps-2020-0031.

[17] Khan SA, Shahid S, Shahid B, Fatima U, Abbasi SA. Green synthesis of MnO nanoparticles using abutilon indicum leaf extract for biological, photocatalytic, and adsorption activities. Biomolecules. 2020;10(5):785. doi: 10.3390/biom10050785.

[18] Prasad AS. Green synthesis of nanocrystalline manganese (II, III) oxide. Mater Sci Semicond Process. 2017;71:342–7. doi: 10.1016/j.mssp.2017.08.020.

[19] Hoseinpour V, Ghaemi N. Green synthesis of manganese nanoparticles: Applications and future perspective–A review. J Photochem Photobiol B: Biol. 2018;189:234–43. doi: 10.1016/j.jphotobiol.2018.10.022.

[20] Ding B, Zheng P, Ma PA, Lin J. Manganese oxide nanomaterials: synthesis, properties, and theranostic applications. Adv Mater. 2020;32(10):1905823. doi: 10.1002/adma.201905823.
[21] Veeramani H, Aruguete D, Monsegue N, Murayama M, Dippon U, Kappler A, et al. Low-temperature green synthesis of multivalent manganese oxide nanowires. ACS Sustainable Chem Eng. 2013;1(9):1070–4. doi: 10.1021/sc400129n.
[22] Saod WM, Hamid LL, Alaallah NJ, Ramizy A. Biosynthesis and antibacterial activity of manganese oxide nanoparticles prepared by green tea extract. Biotechnol Rep. 2022;34:e00729. doi: 10.1016/j.btre.2022.e00729.
[23] Wang L, Zhang K, Han S, Zhang L, Bai H, Bao F, et al. Constituents isolated from the leaves of Glycyrrhiza uralansis and their anti-inflammatory activities on LPS-induced RAW264.7 cells. Molecules. 2019;24(10):1923. doi: 10.3390/molecules24101923.
[24] Vu-Quang H, Vinding MS, Nielsen T, Ullisch MG, Nielsen NC, Nguyen DT, et al. Pluronic F127-folate coated super paramagenic iron oxide nanoparticles as contrast agent for cancer diagnosis in magnetic resonance imaging. Polymers (Basel). 2019;11(4):743. doi: 10.3390/polym11040743.
[25] Domínguez-Delgado CL, Fuentes-Prado E, Escobar-Chávez JJ, Vidal-Romero G, Rodríguez Cruz I, Díaz-Torres R. Chitosan and pluronic® F-127: Pharmaceutical applications. Encyclopedia of biomedical polymers and polymeric biomaterials. New York, NY, USA: Taylor and Francis; 2016. p. 1513–35.
[26] Kao TC, Wu CH, Yen GC. Bioactivity and potential health benefits of licorice. J Agric Food Chem. 2014;62(3):542–53. doi: 10.1021/jf404939f.
[27] Boa F, Bai HY, Wu ZR, Yang ZG. Phenolic compounds from cultivated Glycyrrhiza uralensis and their PD-1/PD-L1 inhibitory activities. Nat Prod Res. 2021;35(4):562–9. doi: 10.1080/14786419.2019.1586698.
[28] Siracusa L, Saija A, Cristani M, Cimino F, D Arrigo M, Trombetta D, et al. Phytocomplexes from liquorice (Glycyrrhiza glabra L.) leaves—Chemical characterization and evaluation of their antioxidant, anti-genotoxic and anti-inflammatory activity. Fitoterapia. 2011;82(4):546–56. doi: 10.1016/j.fitote.2011.01.009.s.
[29] Mourdikoudis S, Pallares RM, Thanh NTK. Characterization techniques for nanoparticles: Comparison and complementarity upon studying nanoparticle properties. Nanoscale. 2018;10:12871–934. doi: org/10.1039/C8NR02278J.
[30] Elderdery AY, Alzahrani B, Hamza SMA, Mostafa-Hedeab G, Mok PL, Subbiah SK. CuO-TiO_2-chitosan-berbamine nanocomposites induce apoptosis through the mitochondrial pathway with the expression of P53, BAX, and BCL-2 in the human K562 cancer cell line. Bioinorg Chem Appl. 2022 Sep 17;2022:9602725. doi: 10.1155/2022/9602725. PMID: 36164585; PMCID: PMC9509271.
[31] Sharma S, Chauhan P, Husain S. Structural and optical properties of Mn_2O_3 nanoparticles & its gas sensing applications. Adv Mater Proc. 2016;1(2):220–5. doi: 10.5185/amp.2016/220.
[32] Chen H, He J. Facile synthesis of monodisperse manganese oxide nanostructures and their application in water treatment. J Phys Chem C. 2008;112(45):17540–5. doi: 10.1021/jp806160g.
[33] Saravanakumar B, Lakshmi SM, Ravi G, Ganesh V, Sakunthala A, Yuvakkumar R. Electrochemical properties of rice-like copper manganese oxide ($CuMn_2O_4$) nanoparticles for pseudocapacitor applications. J Alloy Compd. 2017;723:115–22. doi: 10.1016/j.jallcom.2017.06.249.
[34] Gnanam S, Rajendran V. Synthesis of CeO_2 or α–Mn_2O_3 nanoparticles via sol–gel process and their optical properties. J Sol-Gel Sci Technol. 2011;58(1):62–9. doi: 10.1007/s10971-010-2356-9.
[35] Arena F, Torre T, Raimondo C, Parmaliana A. Structure and redox properties of bulk and supported manganese oxide catalysts. Phys Chem Chem Phys. 2001;3(10):1911–7. doi: 10.1039/b100091h.
[36] Esfahani RN, Khaghani S, Azizi A, Mortazaeinezhad F, Gomarian M. Facile and eco-friendly synthesis of TiO_2 NPs using extracts of Verbascum thapsus plant: An efficient photocatalyst for reduction of Cr (VI) ions in the aqueous solution. J Iran Chem Soc. 2020;17(1):205–13. doi: 10.1007/s13738-019-01755-7.
[37] Pizzino G, Irrera N, Cucinotta M, Pallio G, Mannino F, Arcoraci V, et al. Oxidative stress: harms and benefits for human health. Oxid Med Cell Longev. 2017;2017:8416763. doi: 10.1155/2017/8416763.
[38] Tinoco G, Warsch S, Glück S, Avancha K, Montero AJ. Treating breast cancer in the 21st century: Emerging biological therapies. J Cancer. 2013;4:117–32. doi: 10.7150/jca.4925.
[39] Senapati S, Mahanta AK, Kumar S, Maiti P. Controlled drug delivery vehicles for cancer treatment and their performance. Signal Transduct Target Ther. 2018;3(1):1–19. doi: 10.1038/s41392-017-0004-3.
[40] Sung YK, Kim SW. Recent advances in polymeric drug delivery systems. Biomater Res. 2020;24(1):1–12. doi: 10.1186/s40824-020-00190-7.
[41] Zhang H, Chen WR, Huang CH. Kinetic modeling of oxidation of antibacterial agents by manganese oxide. Environ Sci Technol. 2008;42(15):5548–54. doi: 10.1021/es703143g.
[42] Matsufuji M, Nagamatsu Y, Yoshimoto A. Protective effects of bacterial glyceroglycolipid M874B against cell death caused by exposure to heat and hydrogen peroxide. J Biosci Bioeng. 2000;89(4):345–9. doi: 10.1016/s1389-1723(00)88957-4.
[43] Haneefa MM. Green synthesis characterization and antimicrobial activity evaluation of manganese oxide nanoparticles and comparative studies with salicylalchitosan functionalized nanoform. Asian J Pharm. 2017;11(1):65–74.
[44] Mostafavi E, Zarepour A, Barabadi H, Zarrabi A, Truong LB, Medina-Cruz D. Antineoplastic activity of biogenic silver and gold nanoparticles to combat leukemia: Beginning a new era in cancer theragnostic. Biotechnol Rep. 2022;34:e00714.
[45] Radini IA, Hasan N, Malik MA, Khan Z. Biosynthesis of iron nanoparticles using Trigonella foenum-graecum seed extract for photocatalytic methyl orange dye degradation and antibacterial applications. J Photochem Photobiol B: Biol. 2018;183:154–63. doi: 10.1016/j.jphotobiol.2018.04.014.
[46] Gregoriou Y, Gregoriou G, Yilmaz V, Kapnisis K, Prokopi M, Anayiotos A, et al. Resveratrol loaded polymeric micelles for theranostic targeting of breast cancer cells. Nanotheranostics. 2021;5(1):113–24. doi: 10.7150/ntno.51955.
[47] Gebreslassie YT, Gebretnsae HG. Green and cost-efective synthesis of tin oxide nanoparticles: A review on the synthesis methodologies, mechanism of formation, and their potential applications. Nanoscale Res Lett. 2021;16:97. doi: 10.1186/s11671-021-03555-6.
[48] Balakrishnan S, Mukherjee S, Das S, Bhat FA, Singh PR, Patra CR, et al. Gold nanoparticles-conjugated quercetin induces apoptosis via inhibition of EGFR/PI3K/Akt-mediated pathway in breast cancer cell lines (MCF-7 and MDA-MB-231). Cell Biochem Funct. 2017;35(4):217–31. doi: 10.1002/cbf.3266.
[49] Ryan L, O Callaghan YC, O Brien NM. The role of the mitochondria in apoptosis induced by 7beta-hydroxycholesterol and cholesterol-5beta, 6beta-epoxide. Br J Nutr. 2005;94:519–25. doi: 10.1079/bjn20051524.
[50] Rotem R, Heyfets A, Fingrut O, Blickstein D, Shaklai M, Flescher E. Jasmonates: Novel anticancer agents acting directly and selectively

on human cancer cell mitochondria. Cancer Res. 2005;65:1984–93. doi: 10.1158/0008-5472.CAN-04-3091.

[51] Alhadlaq HA, Akhtar MJ, Ahamed M. Different cytotoxic and apoptotic responses of MCF-7 and HT1080 cells to MnO_2 nanoparticles are based on similar mode of action. Toxicology. 2019;411:71–80. doi: 10.1016/j.tox.2018.10.023.

[52] Xiong S, Chng WJ, Zhou J. Crosstalk between endoplasmic reticulum stress and oxidative stress: A dynamic duo in multiple myeloma. Cell Mol Life Sci. 2021;78(8):3883–906. doi: 10.1007/s00018-021-03756-3.

[53] Daniluk K, Kutwin M, Grodzik M, Wierzbicki M, Strojny B, Szczepaniak J, et al. Use of selected carbon nanoparticles as melittin carriers for MCF-7 and MDA-MB-231 human breast cancer cells. Materials (Basel). 2020;13(1):90. doi: 10.3390/ma13010090.

[54] Majani SS, Sathyan S, Manoj MV, Vinod N, Pradeep S, Shivamallu C, et al. Eco-friendly synthesis of MnO_2 nanoparticles using Saraca asoca leaf extract and evaluation of in vitro anticancer activity. Curr Res Green Sustainable Chem. 2023;6:100367. doi: 10.1016/j.crgsc.2023.100367.

[55] Lu H, Zhang X, Khan SA, Li W, Wan L. Biogenic synthesis of MnO2 nanoparticles with leaf extract of viola betonicifolia for enhanced antioxidant, antimicrobial, cytotoxic, and biocompatible applications. Front Microbiol. 2021;12:761084. doi: 10.3389/fmicb.2021.761084.

[56] Reddy P, Pradeep S, Gopinath SM, Ramu R, Kollur SP, Shivamallu C. Anti-breast cancer potential of MnO_2 nanoparticles using *Terminalia chebula* fruit extract against MCF-7 cell line through in vitro cell cycle and apoptotic studies. Mater Today: Proc. 2022;62:5526–32. doi: 10.1016/j.matpr.2022.04.330.

[57] Srinivasa C, Kumar SRS, Pradeep S, Prasad SK, Veerapur R, Ansari MA, et al. Eco-Friendly synthesis of MnO2 nanorods using gmelina arborea fruit extract and its anticancer potency against MCF-7 breast cancer cell line. Int J Nanomed. 2022 Feb 25;17:901–7. doi: 10.2147/IJN.S335848. PMID: 35250266; PMCID: PMC8888196.

[58] Li Y, Chen L, Chan TH, Liu M, Kong KL, Qiu JL, et al. SPOCK1 is regulated by CHD1L and blocks apoptosis and promotes HCC cell invasiveness and metastasis in mice. Gastroenterology. 2013;144:179–91. doi: 10.1053/j.gastro.2012.09.042.

[59] Moghaddam AB, Moniri M, Azizi S, Rahim RA, Ariff AB, Navaderi M, et al. Eco-friendly formulated zinc oxide nanoparticles: Induction of cell cycle arrest and apoptosis in the MCF-7 cancer cell line. Genes (Basel). 2017;8(10):281. doi: 10.3390/genes8100281.

[60] Vaja F, Guran C, Ficai D, Ficai A, Oprea O. Cytotoxic effects of ZnO nanoparticles incorporated in mesoporous silica. UPB Sci Bull. 2014;76:55–66.

[61] Faheem MM, Bhagat M, Sharma P, Anand R. Induction of p53 mediated mitochondrial apoptosis and cell cycle arrest in human breast cancer cells by plant mediated synthesis of silver nanoparticles from Bergenia ligulata (Whole plant). Int J Pharm. 2022;619:121710. doi: 10.1016/j.ijpharm.2022.121710.